Effect of re-lasing on the fatigue properties of 316L Stainless Steel Produced by laser powder bed fusion

Foued Abroug, Yunran Ma, Morgane Mokhtari, Lionel Arnaud, Anis Hor, Clément Keller

Available online at www.sciencedirect.com

ScienceDirect

Procedia Structural Integrity 57 (2024) 87–94

Structural Integrity Procedia

www.elsevier.com/locate/procedia

Fatigue Design 2023 (FatDes 2023)

Effect of re-lasing on the fatigue properties of 316L Stainless Steel Produced by laser powder bed fusion

Foued Abroug[a,*], Yunran Ma[a], Morgane Mokhtari[a], Lionel Arnaud[a], Anis Hor[b], Clément Keller[a]

[a]*Laboratoire Génie de Production (LGP), Université de Toulouse, INP-ENIT, Tarbes, France*
[b]*Institut Clément Ader (ICA), Université de Toulouse, CNRS, ISAE-SUPAERO, Toulouse, France*

Abstract

Despite the great success of the metal additive manufacturing process by Laser Fusion on Powder Bed (L-PBF), this technique still lacks maturity in several areas. Among its major challenges, the low fatigue strength of the L-PBF parts is caused, among other features, by two main types of defects. Firstly, the L-PBF process generates a high surface roughness, mainly linked to the phenomenon of partial powder melting on the part surface. Secondly, internal defects are created during the building process and are randomly distributed in the material. The present study investigates the effect of a second lasing on the improvements of the surface roughness, defects population as well as fatigue properties of L-PBF parts. Based on preliminary experiments, two re-lasing strategies were selected. A high cycle fatigue campaign was subsequently carried out with a stress ratio of R= -1 on samples with or without re-lasing, in the as-built state or after polishing. Specimens printed in Net-Shape showed even after re-lasing and polishing, a much lower fatigue strength than those machined in the bulk after additive manufacturing. In addition, results show that the tested re-lasing conditions has a beneficial effect on the quasi-static and fatigue strength of the 316L obtained by L-PBF.

Keywords: L-PBF metal additive manufacturing, re-lasing, mechanical properties, high cycle fatigue.

10.1016/j.prostr.2024.03.011

1. Introduction

Metal additive manufacturing is a rapidly expanding field of research and innovation. On one hand, within this technological field, the Laser Powder Bed Fusion technique by (LPBF) occupies a central place because of its ability to generate parts of great geometric complexity in a "near net shape" form, that cannot be achieved with conventional techniques [1]. On the other hand, among the major challenges encountered by L-PBF technique is the high surface roughness of printed parts, mainly related to the phenomenon of melting powders by the laser beam [2]. In addition, internal defects are often created during printing and are randomly distributed in the material [3]. These defects such as porosity and lack of fusion, in addition to surface roughness, reduce drastically the high cycle fatigue strength of L-PBF parts [4]. To overcome these limitations, post-processing steps of different natures can be applied to improve one or more integrity parameters of L-PBF parts (machining, HIP, pickling, laser polishing, etc.) [5]. Such post processes however, are often costly, time consuming and not always applicable in the case of complex geometries where many surfaces are inaccessible [6]. Literature studies have also proposed the application of re-lasing during the building of the part to reduce surface roughness and increase density by closing internal pores [7][8]. This technique seems interesting and in the majority of the studied cases, fruitful. For instance, Yasa et al.[8] reported that re-lasing allows to suppress the stair effect on the 316L L-PBF parts and that applying three re-lasings on each layer of leads to over 99.9% of material density. Another study conducted by Keller et al. [9] on a nickel-based superalloy (Hastelloy X) has shown that a second lasing results in an increase in the part's ductility. The impact of such a technique on the fatigue strength of L-PBF parts is yet to be explored. To our knowledge, no study has been published yet on this subject.

In this study, the effect of a second lasing on the characteristics of parts made by L-PBF is addressed. Different releasing parameters were applied and the samples were assessed. The first objective is to identify the suitable re-lasing parameters to improve the density, surface roughness, and hardness of the parts. Then, the second objective is to identify the potential gain in terms of mechanical characteristics, in quasi-static and in fatigue at a large number of cycles, for the most promising configurations.

2. Material and experimental procedure

2.1. Material and manufacturing conditions

The material studied in this paper is the AISI 316L which is an austenitic stainless steel widely used in various industrial applications due to its corrosion resistance, mechanical properties and formability. All studied parts are made by L-PBF process, using a 3D Systems ProX DMP 300 machine at the CEF3D additive manufacturing platform of ENIT. The powder used is characterized by a D10, D50 and D90 of 9.8, 20.1 and 38.1 µm respectively. The reference building parameters, corresponding to the part built without re-lasing, are shown in Table 1.

Table 1. Reference L-PBF manufacturing parameters.

Sample	P (W)	V (mm/s)	H (µm)	Lt (µm)	Ev (J/mm^3)	Rotating angle (°)
1: reference	215	1800	50	40	59.72	67

In addition to the reference part, 12 parts are built using different re-lasing parameters as shown in Table 2. The built geometries are cylinders of 16 mm in diameter and 10 mm in height. For the sake of simplicity, the re-lasing is applied on the total section of each layer of the printed parts, after powder is melted using the reference parameters. Only the parameters of Power (P), scanning Velocity (V) or Hatch distance (H) were modified, one parameter at a time, in order to obtain comparable energy densities (Ev). The layer thickness (Lt) was however unchanged for this study (see Table 2). Only two configurations were selected to be tested further, in addition to the reference configuration (sample 1).

Table 2. Re-lasing parameters: presented in percentage in comparison to the reference parameters used for sample 1. Blue color indicates the selected parameters for the mechanical testing campaign.

Sample	2	3	4	5	6	***7***	8	***9***	10	11	12	13
Re-lasing Ev (%)	20	40	50	60	70	***80***	90	***100***	60	80	60	80
Modified parameter	*P*	*P*	*P*	*P*	*P*	***P***	*P*	***P***	*V*	*V*	*H*	*H*
Value (%)	20	40	50	60	70	***80***	90	***100***	167	125	176	125

2.2. Mechanical testing

Monotonic tensile tests were performed with an electromechanical Instron 5892 tensile machine with a cross-head displacement control mode (2 mm/min leading to an approximative strain rate of 2×10^{-3} s^{-1}). Deformation was measured with a video extensometer. Three samples were tested for each configuration.

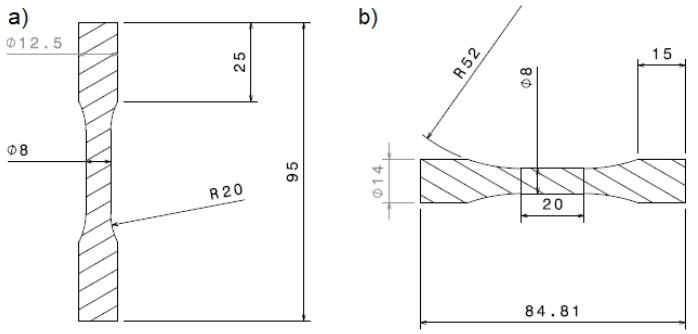

Fig. 1. Sample geometry for (a) monotonic tensile tests and (b) fatigue tests.

Fatigue tests were conducted on samples in the as-built state or after polishing with grinding paper, going from 360 to 2500 grades. For each condition, 3 samples were tested, making a total of 18 tested samples. The tests were conducted under fully reversed (R= -1) tension compression loads, using a servo-hydraulic Instron 8801 machine, at room temperature, at ambient air and at a frequency of 15 Hz. The Locati method is applied as detailed in the work of Maxwell and Nicholas [10], with 3 samples per batch and a loading step of 25 MPa. All samples were tested until failure or until 10^6 cycles are reached. At the end of the fatigue tests, an equivalent fatigue stress is calculated for each sample by accounting for the accumulated damage during the loading steps using Miner's Law [11] combined with Basquin's Law (see equations 1 to 3). A mean fatigue strength per batch is then determined. The samples geometries for monotonic and fatigue tests are shown in Figure 1.

$$\sigma_a = C\, N^{-1/b} \tag{1}$$

$$D = \sum_{i=1}^{m} D_i = \sum_{i=1}^{m} \frac{n_i}{N_i} \leq 1 \tag{2}$$

$$D = \sum_{i=1}^{m} n_i \left(\frac{\sigma_a}{C}\right)^b \leq 1 \tag{3}$$

With n_i : number of cycles for each step, σ_a the stress amplitude, D the accumulated damage which equals 1 when the specimen breaks, m the number of steps undergone by the sampled, b and C are material parameters that describe the Wöhler curve of the studied material.

3. Results

3.1. Results of parametric study

The samples detailed in Table 1 and Table 2 were manufactured to determine the impact of re-lasing on the characteristics of the built samples, compared to the reference sample. The assessed characteristics are firstly the density, in terms of the reduction of the percentage of porosity, and the reduction of the population of largest defects, known to be critical for the High Cycle Fatigue (HCF) life. Based on the study of Abroug et al. [12], a particular attention is accorded to the population of defects having a $\sqrt{area}$ larger than 20 µm. health matter was checked using optical micrography. Secondly, the surface roughness of the 13 parts is assessed after being scanned via the ALICONA Infinite Focus G5 profilometer, both on the top and lateral surface of the parts. Finally, Vickers hardness was measured using Zwick/Roell ZHV2.5 equipment with a 10 kg load (Hv10). All tests were performed using the EN ISO 6507-1 norm. An average of 5 indents were taken on each of the XY, XZ and YZ planes. Results of the assessment of these properties are shown in Table 3 And Figure 2.

Table 3. Results of properties assessment for the 13 samples. Blue color indicates the properties of the selected configurations for the mechanical testing campaign.

Sample	1	2	3	4	5	6	*7*	8	*9*	10	11	12	13
Hardness (Hv10)	225.8	231.3	230.3	222.1	234.7	230.9	*234.7*	232.7	*233.3*	233.3	225.3	233.0	228.3
Sa (Lateral) (µm)	15.9	14.9	15.8	16.6	14.1	14.5	*13.1*	14.1	*12.6*	14.3	17.5	11.3	15.8
Sa (Top) (µm)	9.7	9.3	9.7	9.9	9.0	9.3	*8.0*	8.2	*8.9*	9.8	10.4	13.4	9.2

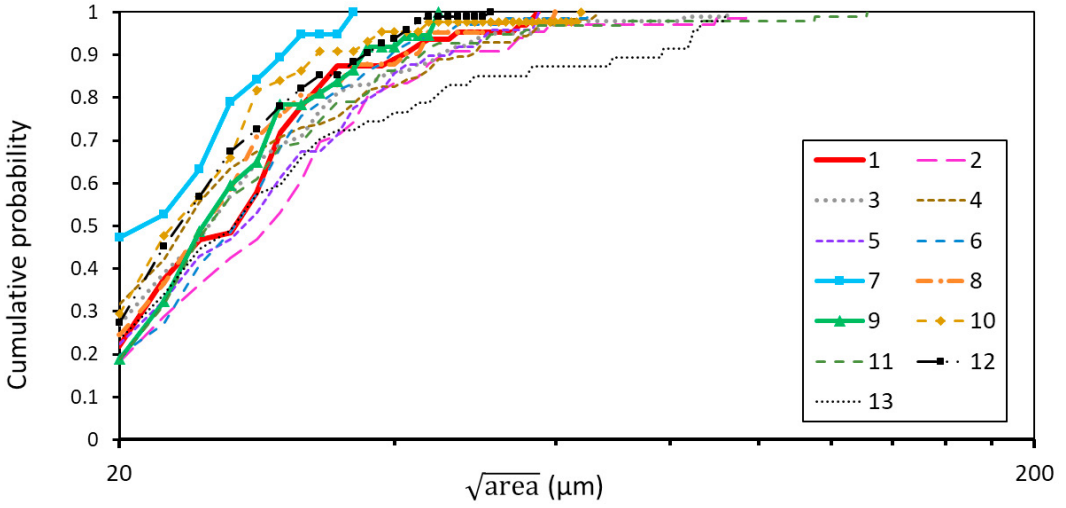

Fig. 2. Average fatigue strength obtained by batch.

Conditions 7 and 9 (respectively a re-lasing with a power of 80% and 100%) were selected because they combined the most optimized properties. First, Initial density, obtained for sample 1, reached >99% and rescanning doesn't seem to have a large effect on the global porosity. Indeed, as a high-density level is already reached by the initial scanning, it is difficult to significantly improve it by re-lasing. However, configurations 7 and 9 enable porosity decrease as well as decrease of the number of large pores, having a $\sqrt{area}$ larger than 20 µm, by about half (lines blue and green on Figure 2). Samples 7 and 9 also exhibit the lowest lateral surface roughness among the 13 tested samples, as well as a slightly improved hardness, compared to the reference sample 1 (see Table 3). Both configurations were hence selected to produce the batches used for mechanical testing. Other configurations allowed also a reduction in terms of

density, number of large pores as well as lateral surface roughness, such as configurations 10 and 12. Sample 12 actually showed better results than sample 9 in terms of lateral surface roughness and defects healing, its top surface roughness however was the highest among all samples (see Table 3). As for sample 10, its top and lateral surface roughness values were higher than those of samples 7 and 9. All other samples showed higher number of large pores than the reference sample as well as higher surface roughness than samples 7, 9 and in some cases sample 1.

3.2. Results of mechanical testing

Monotonic tensile tests allowed to identify the effect of re-lasing in enhancing the monotonic properties of the 316L L-PBF parts. Engineering strain-stress curves were recorded and plotted in Figure 3. Significant change between the reference and the re-lased samples was observed. For the conditions 7 (re-lasing with P= 80%) only two curves could be recorded. First, one can observe a good reproducibility of test results. All samples showed an elasto-plastic behavior with large ductility. From the curves the effect of re-lasing is visible as samples show a lower strain hardening and a higher elongation at break than reference configuration samples (see Table 4). Ductility is hence significantly changed due to the change of the necking strain (ε_N) and fracture strain (ε_F) values. However, the influence of re-lasing power is not significant except for a slightly higher elongation for the configuration 9 samples over the configuration 7 samples. Based on these results and the hardness measurements results, a higher fatigue strength could be expected for re-lased samples compared to the non re-lased ones.

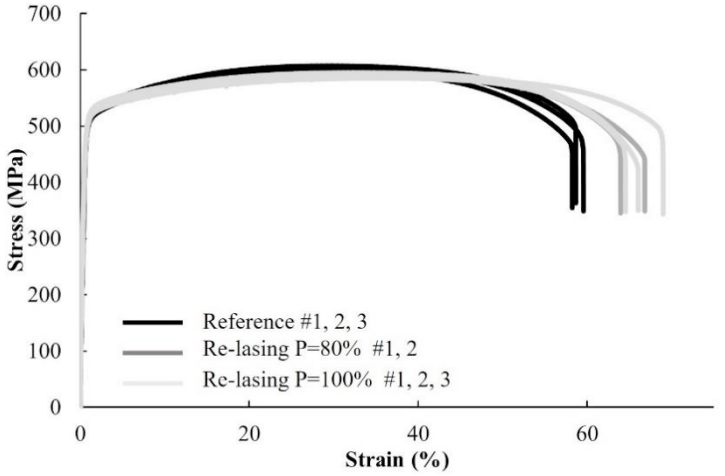

Fig. 3. Stress–strain tensile curves of reference and re-lased samples (configuration 7 (P=80%) and 9 (P=100%)).

Table 4: Tensile properties of the reference and re-lased samples from configuration 7 (P=80%) and 9 (P=100%).

configuration	YS (MPa)	UTS (MPa)	ε_N (%)	ε_F (%)
1: Reference	475±13	602±5	28±1	58±1
7: Rescanning P=80%	473±2	594±1	31±1	64±2
9: Rescanning P=100%	478±10	590±5	33±1	66±2

3.3. Results of fatigue testing

As for the high cycle fatigue tests, the results of fatigue strength, presented in terms of σ_D, are shown in Figure 4 and allow to draw several conclusions. Firstly, fatigue results show, for the polished and the as-built batches, a slight enhancement after re-lasing. For the As-built state, the average fatigue strength increases and by 3% after re-lasing at 80% of laser power (configuration 7 and as-built batch named R80_AB) and by 8%, after re-lasing at 100% of laser power (configuration 9 and as-built batch named R100_AB). As for after polishing, the average fatigue strength

increased by 5% after re-lasing at 100% of laser power (configuration 9 and polished named R100_P) batch and by 19% after re-lasing at 80% of laser power (configuration 7 and polished batch named R80_P). In addition, polishing allowed to increase fatigue strength compared to the As-built state. For instance, the reference batch gained 6% of fatigue strength after polishing (non re-lased and polished batch named NR_P) compared to the As-built batch (non re-lased and as-built batch named NR_AB). Compared to the reference batch NR_AB, the best result is obtained for the batch R80_P, after re-lasing at 80% of laser power and polishing, where 26% of fatigue strength increase is noted (see Figure 4).

Furthermore, the scatter of the fatigue strength results was lowest for the R100_P and the R80_AB batches, whereas the batches R100_AB and R80_P showed more scatter in results. This allows to conclude that the re-lasing process, in the conditions tested, doesn't reduce the scatter in fatigue tests. Finally, the tendency of fatigue strength enhancement has changed for the polished and As-built batches, between the configurations 7 and 9. For the As-built state, the R100_AB batch exhibits the best result, whereas after polishing, the R80_P presents the best results.

The fatigue strength values results obtained for the tested samples are much lower than other results from the literature such as those obtained by Merot et al. [13] despite having the same samples geometry and almost the same hardness values. This could be due to the boundary effect that the samples studied in this paper have since they were built in a net shape format, compared to the samples machined in the bulk in Merot's study.

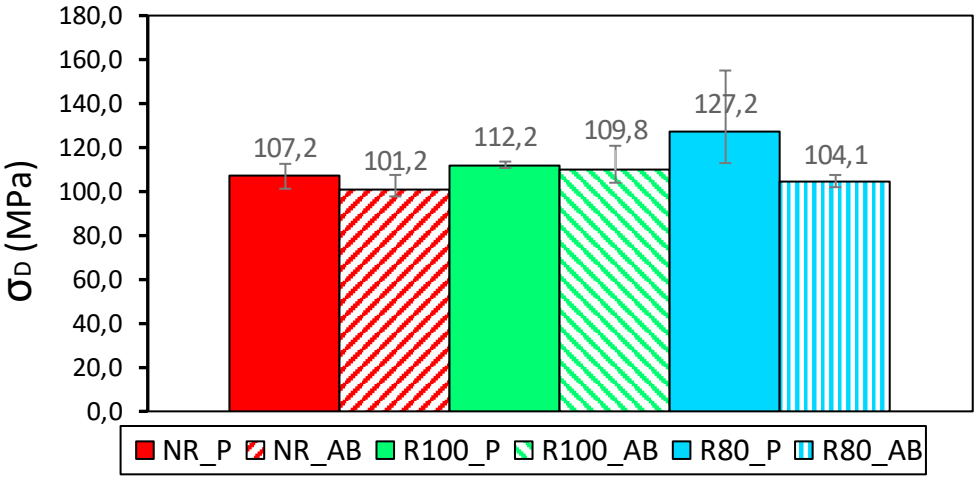

Fig. 4. Average fatigue strength obtained by batch.

For the damage mechanisms, all fatigue failures occurred at the surface of the samples, from lack of fusion (LoF) type defects (see Figure 5). After re-lasing, density of defects is reduced but defects aren't completely erased. LoF defects responsible of fatigue failure reached a $\sqrt{area}$ values of 307µm even after re-lasing.

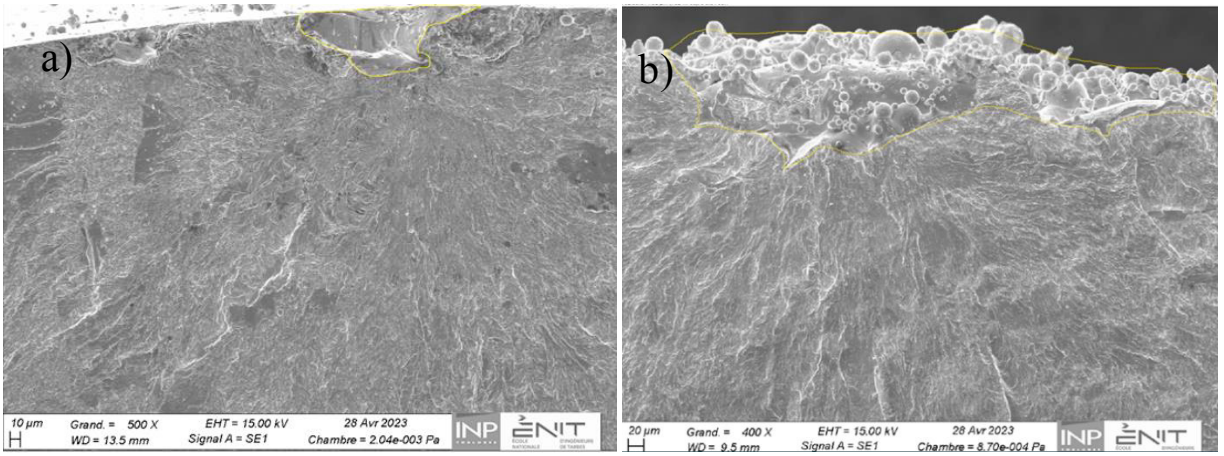

Fig. 5. Crack initiation site of a sample from the a) R80_P batch with a $\sqrt{area}$ of 82 µm and b) R100_AB batch with a $\sqrt{area}$ of 268 µm.

3.4. Kitagawa diagram

Results of the fractographic analysis are shown in terms of Kitagawa diagram in Figure 6. The same colour code than in Figure 4 is used for the different batches. As it can be seen, The Murakami model, detailed in equation 4 and applied using a hardness value of 230 Hv10, allows for a non-conservative evaluation of the fatigue strength, due to the boundary effect mentioned earlier and caused by the net shape form of the parts. As a remedy, a correction factor is applied. The correction factor chosen as 0.5 allows a more accurate description of the observed fatigue behavior.

$$\sigma_D = \frac{1.43\ (H_v+120)}{(\sqrt{area})^{1/6}} \tag{4}$$

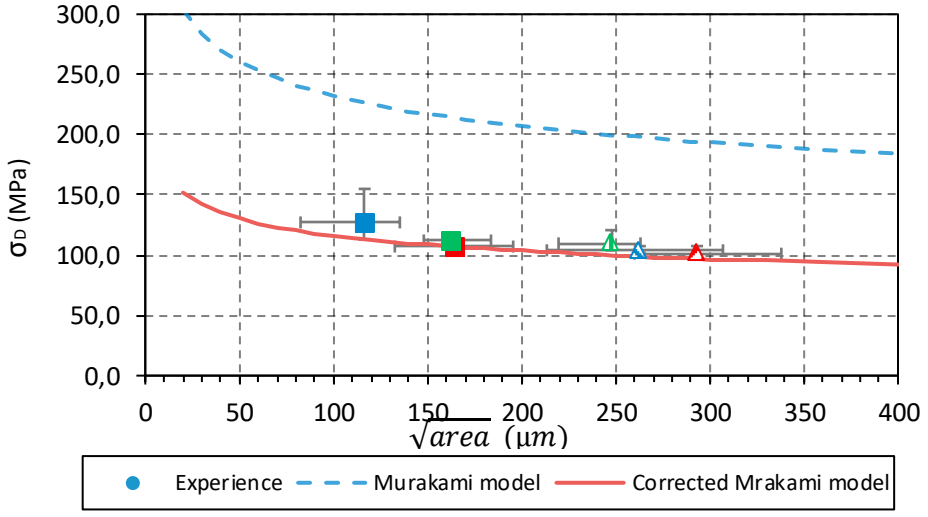

Fig. 6. Kitagawa diagram for the tested batches.

4. Conclusions

The results of this study can be summarized in the following points:

- Among the re-lasing parameters tested, re-lasing with 80% or 100% of laser power (e.g. samples 7 and 9), allowed to improve the material density, hardness as well as lateral and top surface roughness of the L-PBF parts. LoF type defects however, although reduced in population after re-lasing, still exist on the parts.
- Monotonic tensile tests showed that re-lasing allowed a gain of necking strain and fracture strain. The strain hardening however is reduced.
- HCF tests showed that after re-lasing at 80% of laser power and polishing, 26% of fatigue strength increase is obtained compared to the as-built reference batch. The obtained fatigue strength values however, are far less than those for samples machined at the bulk after additive manufacturing. This is due to the net shape effect.
- All crack initiation occurred at LoF defects at the surface, even after re-lasing. The Murakami criterion allowed, after accounting for the net-shape effect, to describe correctly the observed fatigue behavior.

As a perspective, the effect of re-lasing on the microstructure of the L-PBF parts should be examined. Also, other promising re-lasing techniques could be tested and their effect on the fatigue life assessed. Furthermore, the transition in fatigue strength between machined samples and net shape samples needs to be further explored in order to be better accounted for in the fatigue design of L-PBF parts.

Acknowledgments

The authors would like to acknowledge J. Pécune, N. Aubazac, Y. Balcaen, V. Lagarde and B. Lorrain for the technical support in terms of material analysis and mechanical testing, A. Vezirian for producing SLM samples and J. Alexis for his helpful discussions.

References

[1] B.Verquin, S. Hoguin, 2019, «Metal additive manufacturing – The essentials. » Centre technique des industries mécaniques (Cetim).
[2] Santecchia, E., Spigarelli, S., & Cabibbo, M. (2020). Material reuse in laser powder bed fusion: Side effects of the laser—metal powder interaction. Metals, 10(3), 341.
[3] Zhang, B., Li, Y., & Bai, Q. (2017). Defect formation mechanisms in selective laser melting: a review. Chinese Journal of Mechanical Engineering, 30, 515-527.
[4] Zhang, M., Sun, C. N., Zhang, X., Goh, P. C., Wei, J., Hardacre, D., & Li, H. (2017). Fatigue and fracture behaviour of laser powder bed fusion stainless steel 316L: Influence of processing parameters. Materials Science and Engineering: A, 703, 251-261.
[5] Khan, H. M., Karabulut, Y., Kitay, O., Kaynak, Y., & Jawahir, I. S. (2020). Influence of the post-processing operations on surface integrity of metal components produced by laser powder bed fusion additive manufacturing: a review. Machining Science and Technology, 25(1), 118-176.
[6] Duval-Chaneac, M. S., Han, S., Claudin, C., Salvatore, F., Bajolet, J., & Rech, J. (2018). Experimental study on finishing of internal laser melting (SLM) surface with abrasive flow machining (AFM). Precision Engineering, 54, 1-6.
[7] Liang, A., Hamilton, A., Polcar, T., & Pey, K. S. (2022). Effects of rescanning parameters on densification and microstructural refinement of 316L stainless steel fabricated by laser powder bed fusion. Journal of Materials Processing Technology.
[8] Yasa, E., & Kruth, J. P. (2011). Microstructural investigation of Selective Laser Melting 316L stainless steel parts exposed to laser re-melting. Procedia Engineering, 19, 389-395.
[9] Keller, C., Mokhtari, M., Vieille, B., Briatta, H., & Bernard, P. (2021). Influence of a rescanning strategy with different laser powers on the microstructure and mechanical properties of Hastelloy X elaborated by powder bed fusion. Materials Science and Engineering: A, 803, 140474.
[10] Maxwell DC, Nicholas T. A rapid method for generation of a haigh diagram for high cycle fatigue. In: Fatigue and Fracture Mechanics: 29th Volume. ASTM International. 1999.
[11] Miner MA. Cumulative damage in fatigue. J Appl Mech Trans ASME 1945;12:159–64.
[12] Abroug, F., Monnier, A., Arnaud, L., Balcaen, Y., & Dalverny, O. (2022). High cycle fatigue strength of additively manufactured AISI 316L Stainless Steel parts joined by laser welding. Engineering Fracture Mechanics, 275, 108865.
[13] Merot, P., Morel, F., Mayorga, L. G., Pessard, E., Buttin, P., & Baffie, T. (2022). Observations on the influence of process and corrosion related defects on the fatigue strength of 316L stainless steel manufactured by Laser Powder Bed Fusion (L-PBF). IJF, 155, 106552.